Trop J Nat Prod Res, April 2023; 7(4):2926-2934 ISSN 2616-0684 (Print)
ISSN 2616-0692 (Electronic)

Tropical Journal of Natural Product Research

Available online at https://www.tjnpr.org

*Original Research Article*

# Optimizing the Synthesis of Silver Nanoparticles Using Five Curcuma Species under UV Irradiation as a Potent Suncreen Substrate

Wisnu Widikdo[1], Purwantiningsih Sugita[1]*, Mohammad Khotib[1], Witta K. Restu[2], Rahmayeni Rahmayeni[3], Harry Agusnar[4]

[1]*Department of Chemistry, Faculty of Mathematics and Natural Sciences, IPB University, Bogor 16680, Indonesia;*
[2]*Research Center for Chemistry, National Research and Innovation Agency (BRIN) Kawasan Puspiptek Serpong, Tangerang Selatan 15314, Banten, Indonesia;*
[3]*Department of Chemistry, Faculty of Mathematics and Natural Sciences, Andalas University, 25163, Indonesia*
[4]*Department of Chemistry, Faculty of Mathematics and Natural Sciences, University of Sumatera Utara, Medan 20222, Indonesia*.

ARTICLE INFO

*Article history:*
Received 18 March 2023
Revised 16 March 2023
Accepted 17 April 2023
Published online 01 June 2023



ABSTRACT

Curcuma rhizome is reported to have a high total phenolics that could act as reducing agents for metals to nanoparticles. Rhizomes of five curcuma species were selected as bioreductors, namely white turmeric (*Curcuma zedoaria*), black turmeric (*C. aeruginosa*), fingerroot (*C. rotunda*), temu giring (*C. heyneana*), and mango ginger (*C. amada*). The research was designed to select the reductor from five *Curcuma* rhizomes mentioned above for silver nanoparticles synthesis, optimizing the synthesis condition, and evaluating its potential as a sunscreen agent. Silver nanoparticles (AgNPs) were synthesized by mixing the extracts with $AgNO_3$ and irradiating the solution under a 366 nm UV lamp at certain times and pHs. Based on the spectra, the highest absorbance of silver nanoparticles was detected on the temu kunci extract. The optimum conditions for silver nanoparticle-temu kunci (AgNPs-TK) were determined using a Box-Behnken Design and Minitab. Statistical results showed that 0.13 g of silver nitrate irradiated for 162.7 min at pH 11.34 was the optimum condition for AgNPs synthesis. The synthesized AgNPs were characterized by PSA/DLS, XRD, and TEM. The TEM analysis confirmed that silver particles are spherical. The size of the AgNPs produced based on TEM analysis is 5–50 nm. Sunlight inhibition activity, determined spectrophotometrically, indicated that the sun protection factor of AgNPs-TK is categorized as a minimum protection in concentration of 25 ppm.

***Keywords***: Box-Behnken Design, fingerroot extract, Silver nanoparticles, Sun Protection Factor, UV irradiation .

## Introduction

Nanotechnology is currently the field of manufacturing that is expanding rapidly, and scientists are working eagerly to create new nanomaterials and manufacturing processes. It is a significant area of contemporary research that deals with synthesizing, constructing, and manipulating particle structures with sizes ranging from 1 to 100 nm.[1] Novel uses of nanoparticles and nanomaterials are rapidly expanding in various fields due to their new or better applications because of their size, dispersion, and shape.[2] However, the production of nanoparticles often entails several problems: such as high cost, potentially damaging chemical and physical processes that use hazardous and poisonous substances that pose various biological risks.

Silver nanoparticles (AgNPs) have recently gained much interest from academics across many different sectors due to their unique features and the broad spectrum of applications, including in food science, medicine, agriculture, and agricultural technology.[3] Numerous research has demonstrated the antioxidant,[4,5] antibacterial,[6,7] anticancer,[8,10] antifungal,[11,12] antileshmanial,[13] photocatalytic,[14] sensor,[15] wound healing,[16] and other properties of silver nanoparticles.

*Corresponding author. E mail: purwantiningsih@apps.ipb.ac.id
Tel: +62 818686194

**Citation:** Widikdo W, Sugita P, Khotib M, Restu WK, Rahmayeni R, Agusnar H. Optimizing the Synthesis of Silver Nanoparticles Using Five Curcuma Species under UV Irradiation as a Potent Suncreen Substrate. Trop J Nat Prod Res. 2023; 7(4):2926-2934 http://www.doi.org/10.26538/tjnpr/v7i5.13

Official Journal of Natural Product Research Group, Faculty of Pharmacy, University of Benin, Benin City, Nigeria.

AgNPs can be produced using a variety of techniques, including physiochemical methods,[17] sonoelectrochemical synthesis,[18] microemulsion technique,[19] photochemical synthesis,[20] microwave-based systems,[21] radiation,[22,23] and most recently, a green synthesis method. Many of these physiochemical approaches are robust and theoretically feasible. Still, their practical application is severely constrained by dangerous chemicals, high costs, high energy and time requirements, and problems with waste purification. As a result, the nanosilver synthesis technique increasingly needs cost-effective, eco-friendly, and cost-efficient synthesis approaches that use non-toxic chemicals. An alternative is the natural, environmentally safe, and biocompatible production of AgNPs utilizing a variety of plants, microorganisms, and algae.[3] AgNPs have the potential to protect the skin from UV light. Ho *et al*.[24] reported that AgNPs have an ability comparable to titanium oxide in protecting human keratinocyte cells from UV-B light. Palanki *et al*.[25] reported that AgNPs in a size range of 10–40 nm were completely efficient in protecting keratinocyte cells (HaCaT) from UVB-induced apoptosis.

Creating experimental techniques for synthesizing nanoparticles with natural inspiration is a crucial field of nanotechnology. The utilization of plants as the production assembly of AgNPs has attracted interest; there have been numerous reports of plants that make it easier to produce them. Plants and their parts contain primary metabolites such as carbohydrates, fats, proteins, nucleic acids, pigments, and several types of secondary metabolites (terpenoids, saponins, phenolics, alkaloids), which can reduce and stabilize silver ions, although they have chemical complex structures but environmentally safe and already recognized to have therapeutic value in plant extracts.[26,27,28] *Curcuma* is an economically significant genus with numerous applications. Its uses include spices, food preservatives, flavoring agents, pharmaceuticals,

colors, cosmetics, starch, and decorations.[29] Curcuma plants have many activities, such as antibacterial,[30] antiviral,[31] and antifungal activity,[32] and can also be used as a reducing and stabilizing agent. Patra and Kurdi[33] developed curcumin from turmeric as a reducing agent for different metallic nanoparticle preparation such as gold (Au), silver (Ag), copper (Cu), iron (Fe), manganese (Mn), and zinc (Zn). Alsammarraie *et al*.[34] used turmeric (*Curcuma longa*) extract as a reducing agent and capping agent to synthesize AgNPs. The ability of plants as a reducing agent is due to functional molecules such as aldehydes, ketones, carboxylic acids, amides, enzymes, terpenoids, phenols, and flavones.[3] AgNPs synthesis mediated by the genus Curcuma rhizome belonging to the Zingiberaceae extract is still limited. Five species of the Curcuma genus were used in this experiment, namely white turmeric (*C. zedoaria*), black turmeric (*C. aeruginosa*), fingerroot (*C. rotunda*), temu giring (*C. heyneana*), and mango ginger (*C. amada*).

There hasn't been any information about optimal condition for silver nanoparticles synthesis using combination of UV irradiation and *Curcuma* rhizomes mentioned above with their sunlight inhibition activity. In this study, we aimed to optimize the AgNPs synthesized by *Curcuma* rhizomes extract using response surface methodolgy (Box Behnken design) and evaluate their potential as a sunscreen agent material.

## Materials and Methods

*Preparation of curcuma rhizome extract*

The rhizomes of *C. aeruginosa*, *C. amada*, *C. heyneana*, *C. rotunda*, and *C. zedoaria* were obtained by Biopharmaca Conservation and Cultivation Station (BCCS), a technical acting unit under the Biopharmaca Research Center IPB University, Bogor (6° 33' 3.1752" S 106° 43' 31.8108" E), West Java, Indonesia, in January 2019. One hundred grams of mango ginger and temu giring were macerated in ethanol, fingerroot mecerated in acetone, black turmeric and white turmeric were macerated in methanol, each with a ratio of simplicia (g): solvent (mL) 1:3. The suspensions were then filtered and concentrated using a rotary evaporator.

*Selection of extract as the best reducing agent*

Each concentrated rhizome extract (0.2 g) was dissolved in 10 mL of solvent (mango ginger and temu giring were dissolved in ethanol, fingerroot were dissolved in acetone, black turmeric and white turmeric were dissolved in methanol) and mixed with 0.1 g $AgNO_3$ in 90 mL of water. The mixture was added with sodium hydroxide to pH 9 and irradiated using a 366 nm UV lamp for 90 minutes. The absorbance was detected spectrophotometrically from a 380–800 nm wavelength and then centrifuged at 15000 rpm for 15 minutes to precipitate the AgNPs. Then the supernatant was analyzed using atomoc absorption spectrometer (AAS) to determine the remaining Ag ion content. Equation (1) was used to calculate the AgNP's conversion rate.

$$\text{AgNPs Conversion Rate} = 1 - \frac{Concentration\ of\ Ag\ ions\ in\ the\ supernatant\ (ppm)}{Total\ concentration\ of\ Ag\ (ppm)} \times 100\% \quad \text{Equation 1}$$

*Synthesis of AgNPs with fingerroot extract and optimization*

A total of 0.2 g of fingerroot extract was weighed and dissolved in 10 mL of acetone and mixed with $AgNO_3$ in 90 mL of water with variable stated in Table 1 to be optimized by Behnken Design Box (BBD) using Minitab Statistical Software with absorbance response at 430 nm wavelength. Experimental replication was carried out once. The BBD method optimized the AgNPs synthesis parameters to find the highest yield characterized by absorbance at 430 nm wavelength. The three optimized parameters were pH, the mass of $AgNO_3$ used, and the irradiation time under a 366 nm UV lamp (Table 1). Each variable is considered to have three levels (−1, 0, +1). The BBD matrix consisting of 15 trials (involving three variables, each variable at three levels) was obtained using the Minitab Statistical Software (Trial version). The synthesized AgNPs were then diluted ten times with distilled water and analyzed for absorbance spectrophotometrically (Vernier Go Direct Spectrovis Plus) at a wavelength of 430 nm.

*Characterization of Silver Nanoparticles*

The optimized silver-fingerroot (AgNPs-TK) nanoparticle solution was characterized using the Horiba-SZ 100z Particle Size Analyzer (PSA) in ILRC Lab, University of Indonesia. The AgNPs-TK solution was then centrifuged at 15000 rpm (4°C) for 15 minutes, separated from the supernatant and and freeze-dried for further characterization using an an X-ray diffraction (XRD PANalytical AERIS) instrument to evaluate the product's crystallinity. The AgNPs-TK solution that had been centrifuged and redissolved with distilled water was then characterized by Transmission Electron Microscope (Tecnai G2 20S-Twin) to see the morphology and size of the silver nanoparticles formed.

*Measurement of the Sun Protection Factor (SPF) Value of silver*

The experiment refers to *Dutra et al.*[35] with a little modification

A 0.1 g freeze-dried sample was transferred, dissolved in 10 mL ethanol, and homogenized by ultrasonication for 5 minutes. The solution was further diluted to 800, 600, 400, 200, 100, 50, and 25 ppm, in ethanol. The absorption spectrum of the sample in solution was obtained in the range of 290 to 450 nm using a 1 cm quartz cell and ethanol as a blank. Absorption data ranged from 290 to 320 every 5 nm, determined at each point, followed by applying the Mansur equation for the SPF (Equation 2).

$$\text{SPF} = \text{CF} \times \sum_{290}^{320} \text{EE}(\lambda) \times \text{I}(\lambda) \times \text{Abs}(\lambda) \quad \text{Equation 2}$$

EE : Erythemal effect spectrum
I : Solar intensity spectrum
Abs : Absorbance of sunscreen product
CF : Correction factor (= 10)

**Table 1:** Variable for Box Behnken Design

| Factor | Variable | Low | High |
|---|---|---|---|
| A | pH | 7 | 12 |
| B | Mass of $AgNO_3$ (g) | 0.013 | 0.13 |
| C | Irradiation time (minute) | 15 | 240 |

*Statistical analysis*

The MiniTab Statistical Software program (20.3 version, Minitab LLC, PA, US) was used to design and analyze the experiments. Data were analyzed using ANOVA for full quadratic model with a confidence level of 95%.

## Result and Discussion

*Selection of reducing agents from five curcuma rhizomes for the synthesis of silver nanoparticles*

Five curcuma rhizomes, namely white turmeric (*C. zedoaria*), black turmeric (*C. aeruginosa*), fingerroot/temu kunci (*C. rotunda* L.), temu giring (*C. heyneana*), mango ginger (*C. amada*) were used as reducing agents and analyzed spectrophotometrically (Figure 1). The absorbance at a wavelength of 400-450 nm indicates the formation of AgNPs. The absorption at these wavelengths is due to surface plasmon resonance (SPR), a phenomenon in which electrons in the metal surface layer are excited by incident light photons at a certain angle of incidence and then propagate parallel to the metal surface.[36] The absorbance also shows the yields (concentration) of the AgNPs formed. The result is in line with previous findings in which the increase in absorbance is proportional to the yield of the resulting AgNPs.[37] A higher absorbance value indicates a smoother reduction of $Ag^+$ to Ag(0), leading to the quicker and more stable synthesis of the AgNPs.[38] The highest absorbance was shown by AgNPs synthesized using temu kunci (fingerroot) extract. The visible spectrum shows a strong resonance band at a wavelength of around 430 nm. Previous studies have also shown a similar absorbance.[39–41] Based on Figure 1, the most excellent absorbance of the AgNPs formed was in the temu kunci extract, showing that this extract gives AgNPs better than the other four.

AgNPs solutions of the five extracts were further analyzed using an AAS to determine $Ag^+$ content in supernatant (Table 2) and the

proportion (%) of the conversion of $Ag^+$ ions into AgNPs (Figure 2). In this study, the percent conversion of $Ag^+$ into Ag(0) particles with the five curcuma rhizome extracts showed more than 70%, meaning that all extract has the potential as a bioreductor. This low percent conversion may be due to the higher toxicity factor of $Ag^+$ compared to other metal precursors such as $Au^+$, thereby limiting the reduction of $Ag^+$ to Ag(0) facilitated by metabolically obtained reducing agents.[42] Other limiting factors are organic matter such as polysaccharides, cell surfaces, and other biological materials.

*Optimization of AgNPs Synthesis from fingerroot acetone extract*

This study applied the BBD method, and the results were measured regarding absorbance at a wavelength of 430 nm (Table 3). This method has been used to optimize the synthesis of nanoparticles, including AgNPs.[43,44] The BBD method's main advantage is reducing the number of trials[45] by knowing the potential interactions between parameters and saving time by reducing the number of experiments. The response is the absorbance at a wavelength of 430 nm, the surface plasmon response for AgNPs. The results from the BBD table were then analyzed multivariate using linear, 2-factor interaction, and quadratic models (Table 4). The quadratic polynomial model shows the highest *F*- and $R^2$ values and the lowest standard deviation values and *p*-values. The quadratic model delivers the best yield optimization of AgNPs with the mass factor of $AgNO_3$ adjusted for the total phenolic content of temu kunci, pH, and irradiation time under a UV lamp of 366 nm. The quadratic regression model can be written as (Equation 3):

Abs (430 nm) = -7.92 + 1.614 pH + 10.84 mass of $AgNO_3$ + 0.00291 reaction time – 0.0814 pH*pH – 103.3 mass of $AgNO_3$*mass of $AgNO_3$ – 0.000012 reaction time*reaction time + 1.632 pH*mass of $AgNO_3$ + 0.000148 pH*reaction time – 0.0041 mass of $AgNO_3$*reaction time Equation 3

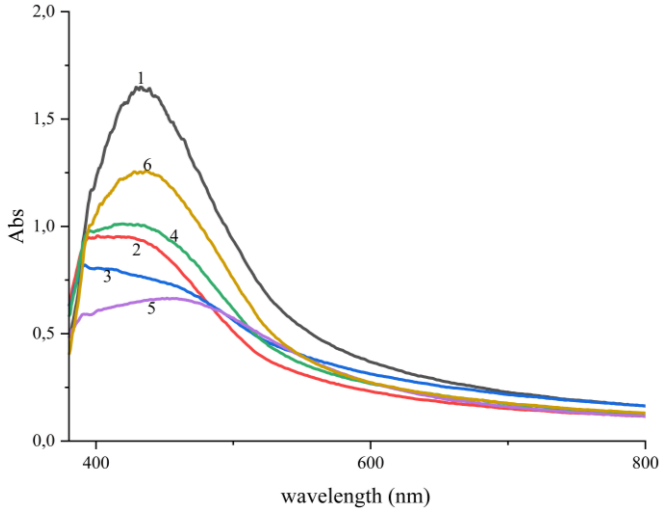


**Figure 1:** Visible spectra of (1) silver-temu kunci/fingerroot (AgNPs-TK) acetone, (2) silver-temu mangga (AgNps-TM) ethanol, (3) silver-temu putih (AgNPs-TP) methanol, (4) silver-temu giring (AgNPs-TG) ethanol, (5) silver-temu hitam ( AgNPs-TH) methanol, and (6) silver-temu kunci (AgNPs-TK) ethanol

The ability of the quadratic model to predict the highest yield of AgNPs was examined by ANOVA. The *F* and *p* values of the model are 34.94 and 0.001, respectively, indicating that the model is significant. A model term with a *p*-value of less than 0.05 is considered substantial. The statistical model of the linear relationship (A, B, and C), the interaction relationship (AB, AC, and BC), and the quadratic relationship ($A^2$, $B^2$, and $C^2$) have a *p*-value of less than 0.05, which illustrates the significance of the statistical model. This case shows that the quadratic polynomial model satisfactorily explains the correlation between AgNPs synthesis and response variables. The lack of fit's *p*-value > 0.10 indicates that the resulting model could be used as a prediction. The model's $R^2$ value (0.9843) shows a good correlation between the predicted and observed values. The predicted $R^2$ values (0.7711) and adjusted $R^2$ values (0.9556) for the synthesis of AgNPs correspond to $R^2$ values (0.9841) close to 1.0, indicating a good model fit in the experimental data (Table 5).

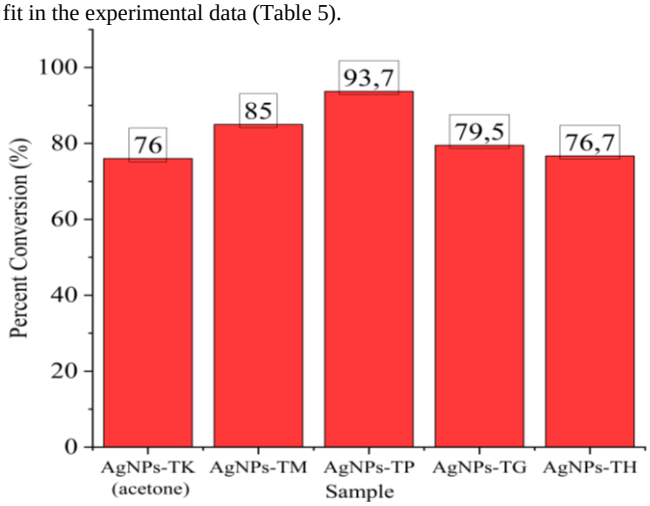


**Figure 2:** The proportion (%) of the conversion of $Ag^+$ ions into AgNPs using five curcuma rhizomes by AAS analysis

**Table 2:** Analysis of $Ag^+$ ion content in supernatant solution using AAS

| Sample | $Ag^+$ ion concentration in supernatant (ppm) |
|---|---|
| AgNPs-TH | 234.09 |
| AgNPs-TM | 115.51 |
| AgNPs-TK | 239.88 |
| AgNPs-TG | 204.71 |
| AgNPs-TP | 62.57 |

The regression equation graphically represents a three-dimensional (3D) response surface plot. Figure 3(a) presents the combined effect of $AgNO_3$ mass and pH on the absorbance at 430 nm while keeping the reaction time at the midpoint and increasing the mass of $AgNO_3$ and pH results in an increase in absorbance. The interactive effect of reaction time and pH on absorbance while keeping the pack of $AgNO_3$ at the midpoint is shown in Figure 3(b). An increase in pH gives an increasing absorbance, and an increase in reaction time gives an increasing absorbance more gently. The combined effect of reaction time and mass of $AgNO_3$ with keeping the pH at the midpoint is depicted in Figure 3(c). Optimization was then carried out with MiniTab software to find the optimum point. The optimum is at the mass of $AgNO_3$ = 0.13 g, pH = 11.34, and reaction time = 162.7 minutes.

Ultraviolet light will help the process of reducing $Ag^+$ ions into AgNPs particles. The photochemical process begins with the reduction of metal precursors from a valence $n^+$ ($Mn^+$) to a zero-valence state [M(0)] by the photocatalytic action of reducing agents.[46] M(0) forms a nucleation center or core, which grows and aggregates to produce nano-sized metal particles. Some of the main advantages of photochemical synthesis are (i) clean process, high spatial resolution, and ease to perform, (ii) controllable preparation of reducing agents *in situ*; nanoparticle formation can be triggered by photo irradiation; and (iii) has high versatility; Photochemical synthesis allows one to manufacture nanoparticles in a variety of media including emulsions, surfactant micelles, polymer films, glasses, cells, and others.[47] The reaction to forming AgNPs under ultraviolet radiation can be written as follows.[48]

$$H_2O \xrightarrow{h\nu} e^-_{aq} + H_3O^+ + H^0 + OH + H_2O_2 \quad (1)$$

$$Ag^+ + e^-_{aq} \xrightarrow{\text{Reduction}} Ag^0 \quad (2)$$

$$Ag^0 + Ag^+ \longrightarrow Ag_2^+ \quad (3)$$

$$Ag^0 + Ag_2^+ \longrightarrow Ag_3^+ \quad (4)$$

**Table 3:** Optimization results with the Box Behnken Design (BBD) method

| Std Order | Run Order | pH (A) | $AgNO_3$ mass (B) | Irradiation time (C) | Abs (430 nm) |
|---|---|---|---|---|---|
| 14 | 1 | 9.5 | 0.0715 | 127.5 | 1.806 |
| 4 | 2 | 12 | 0.13 | 127.5 | 2.113 |
| 11 | 3 | 9.5 | 0.013 | 240 | 0.606 |
| 1 | 4 | 7 | 0.013 | 127.5 | 0.117 |
| 6 | 5 | 12 | 0.0715 | 15 | 1.505 |
| 12 | 6 | 9.5 | 0.13 | 240 | 2.029 |
| 7 | 7 | 7 | 0.0715 | 240 | 0.556 |
| 5 | 8 | 7 | 0.0715 | 15 | 0.442 |
| 15 | 9 | 9.5 | 0.0715 | 127.5 | 1.649 |
| 9 | 10 | 9.5 | 0.013 | 15 | 0.372 |
| 10 | 11 | 9.5 | 0.13 | 15 | 1.902 |
| 3 | 12 | 7 | 0.13 | 127.5 | 0.75 |
| 8 | 13 | 12 | 0.0715 | 240 | 1.785 |
| 13 | 14 | 9.5 | 0.0715 | 127.5 | 1.761 |
| 2 | 15 | 12 | 0.013 | 127.5 | 0.525 |

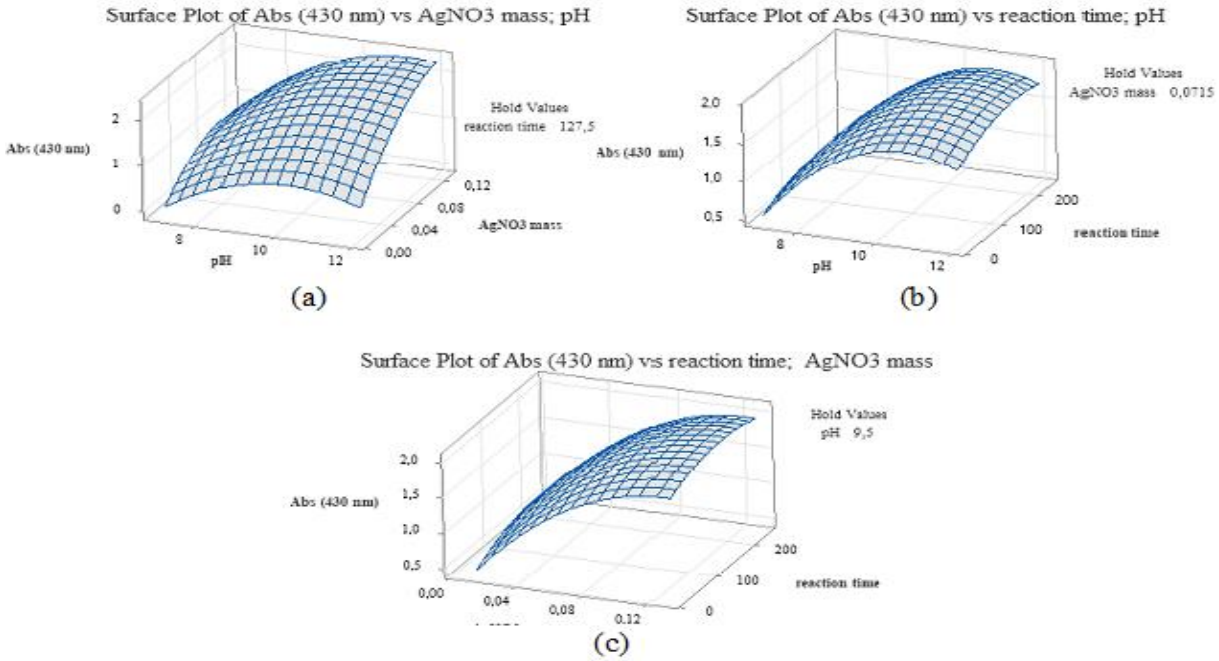


**Figure 3:** Surface Plot (a) Absorbance vs $AgNO_3$ mass; pH, (b) Absorbance vs reaction time; pH, (c) Absorbance vs reaction time; $AgNO_3$ mass

One of the optimizations was carried out by varying the irradiation time of AgNPs under 366 nm UV light. The graph (Figure 3) illustrates an increasing surface plasmon resonance absorbance at an irradiation time of 160 minutes. The absorbance then decreased with the increasing irradiation time. This result can be attributed to the degradation of phenolics under UV irradiation sources.[49] When many phenolics were degraded into small fragments at high irradiation time, some AgNPs that could not be coated with the phenolics clumped into larger particles. Thus, the number of AgNPs decreased, and the intensity of surface plasmon resonance decreased as the absorbance decreased with the time of UV irradiation, indicating that the concentration of AgNPs decreased. Irradiation time can also affect the size of the resulting silver nanoparticles. The following is the mechanism for forming Ag-clusters during UV irradiation.[48,50]

$$(Ag)_n \longrightarrow (Ag)_n^+ + e^-_{aq} \quad (5)$$

$$(Ag)_n^+ + e^-_{aq} \longrightarrow (Ag)_n \quad (6)$$

$$(Ag)_n^+ \longrightarrow (Ag)_{n-1} + Ag^+ \quad (7)$$

**Table 4:** ANOVA Analysis of Box Behnken Optimization

| Source | DF | Adj SS | Adj MS | F-Value | P-Value |
|---|---|---|---|---|---|
| Model | 9 | 7.07659 | 0.78629 | 34.45 | 0.001 |
| Linear | 3 | 5.48103 | 1.82701 | 80.05 | 0.000 |
| pH | 1 | 2.06350 | 2.06350 | 90.41 | 0.000 |
| $AgNO_3$ mass | 1 | 3.34628 | 3.34628 | 146.62 | 0.000 |
| Irradiation time | 1 | 0.07125 | 0.07125 | 3.12 | 0.137 |
| Square | 3 | 1.35780 | 0.45260 | 19.83 | 0.003 |
| pH*pH | 1 | 0.95598 | 0.95598 | 41.89 | 0.001 |
| $AgNO_3$ mass*$AgNO_3$ mass | 1 | 0.46162 | 0.46162 | 20.23 | 0.006 |
| Irradiation time*irradiation time | 1 | 0.09198 | 0.09198 | 4.03 | 0.101 |
| 2-Way Interaction | 3 | 0.23776 | 0.07925 | 3.47 | 0.107 |
| pH* $AgNO_3$ mass | 1 | 0.22801 | 0.22801 | 9.99 | 0.025 |
| pH*irradiation time | 1 | 0.00689 | 0.00689 | 0.30 | 0.606 |
| $AgNO_3$ mass*irradiation time | 1 | 0.00286 | 0.00286 | 0.13 | 0.738 |
| Error | 5 | 0.11412 | 0.02282 | | |
| Lack-of-Fit | 3 | 0.10104 | 0.03368 | 5.15 | 0.167 |
| Pure Error | 2 | 0.01307 | 0.00654 | | |
| Total | 14 | 7.19071 | | | |

**Table 5:** Optimization Parameter of Box Behnken Design

| S | R-sq | R-sq(adj) | R-sq(pred) |
|---|---|---|---|
| 0.151074 | 98.41% | 95.56% | 77.11% |

**Table 6:** Spectrophotometric SPF measurement data from AgNPs

| Concentration (ppm) | SPF Value | Category of protection |
|---|---|---|
| 25 | 7.309 | Minimum |
| 50 | 15.300 | Moderate |
| 100 | 27.884 | Moderate |
| 200 | 58.320 | High |
| 400 | 84.063 | High |
| 600 | 86.687 | High |
| 800 | 86.775 | High |

The above mechanism shows that larger AgNPs are obtained with shorter UV irradiation time and disintegrate due to further UV irradiation. $(Ag)_n$ is a silver nanocluster containing n silver atoms, and $e^-$ aq is an electron in an aqueous solution. Upon UV irradiation of the Ag solution, many electrons are released, and the silver cations are reduced to AgNPs. The nanoparticles also heat up slightly and can anneal th e surrounding surface, causing a slight decrease in size.[51]

Precursor concentration is also one factor affecting the synthesis of AgNPs. Ahmad *et al.*[52] found that an increase in the number of larger nanoparticles was observable when the concentration of silver metal precursor was increased. When the concentration of $AgNO_3$ is relatively high, excess $Ag^+$ will be deposited on the silver metal core, which is formed at the nucleation stage and results in the formation of larger nanoparticles. The shape of AgNPs tends to occur at high pH. The acidic medium creates a driving force that makes the appearance of AgNPs more difficult due to the presence of a repulsive force ($H^+$) to maintain the dispersion of the nanoparticles. Sodium hydroxide in alkaline media dissociates in water to give hydroxide ions ($OH^-$). Negative ions increase the rate of reduction of $Ag^+$ ions to AgNPs. At higher ion densities, Ag atoms tend to diffuse between adjacent adsorption sites on the surface and form bonds with the nearest neighbour atoms via Brownian diffusion[53] due to the high surface energy and thermodynamic instability of the nanoparticle surface, which leads to an increase in particle size.[54]

*Characterization of silver nanoparticles from fingerroot extract*

The synthesized AgNPs-TK under the optimum conditions was characterized. The formation of AgNPs-TK can be proven by the color change from colorless silver ions to brown AgNPs and exhibits a strong surface plasmon resonance absorption band at a wavelength of 400-500 nm (Figure 4). The absorption band is due to the stimulation of free electrons in the outermost orbitals of the AgNPs. Spheroidal AgNPs have a plasmon absorption band of 400–500 nm.[55]

The AgNPs-TK solution was freeze-dried and analyzed using the Fourier Transform Infrared (FTIR) (Figure 5). The spectrum of the fingerroot extract showed absorption bands at wavelengths 2972, 2361, 1706, 1643, 1584, 1448, 1130, and 700 $cm^{-1}$, and broad peaks at of 3400–2400 $cm^{-1}$ indicating the O-H groups in the carboxylic acids. The height at 1706 $cm^{-1}$ confirmed the presence of the carboxylic acid carbonyl (CO) group and was approved by the companying peak at 1448 $cm^{-1}$. Meanwhile, the peaks at 1643 and 1584 $cm^{-1}$ indicate the presence of the C=C group in the conjugated alkene functional group. The rise at 1130 $cm^{-1}$ implies the presence of C-O alcohol. The height at 700 $cm^{-1}$ indicates the presence of C–H groups. The FTIR spectrum on AgNPs-TK gives a slight peak shift; peak intensity decreased/increased and disappeared. A peak at 2971 $cm^{-1}$ with a decreasing intensity indicates the presence of carboxylic acid O–H groups that may be responsible for reducing metal ions into nanoparticles. Some of the peaks shown by the AgNPs-TK spectrum are identical to those of the extract, meaning that the fingerroot extract can function as a capping agent, and the structure of the phenolics in the fingerroot extract is not affected due to interaction with $Ag^+$ ions.

Figure 6(a) exhibits the particle diameters ranging from 93 to 270 nm with an average of 151.3 nm. The polydispersity index of the 0.146 AgNPs solution showed good particle size uniformity. The zeta potential of the AgNPs solution is –58.4 mV. Particles that have a

significant zeta potential value tend to repel each other. The synthesized AgNPs have a negative zeta potential, showing repulsion amongst silver nanoparticles and increasing the nanoparticles' stability. Particles with a zeta potential value more positive than +30 mV or more negative than –30 mV are considered long-term stable.[56] This range will allow the particles to remain in a dispersed form for a longer time, and the attractive forces between Van der Waals particles will not be able to agglomerate the particles. This case also proves that AgNPs are poly-dispersible due to their high negative zeta potential. Electrostatic repulsion between particles prevents nanoparticles' agglomeration and greatly helps long-term stability in the solution.

AgNPs-TK was subjected to X-Ray Diffraction (XRD) analysis (Figure 7). The XRD spectrum shows the crystallinity of the AgNPs. Silver peaks show at 2θ (38.01°, 44.45°, 64.40°, 76.71°) at a half-maximum full-width angle (1.3473, 0.6954, 0.7729, 0.6675) in CuKα radiation (λ=0.15418 Å). The fact is evident from the results that the 2θ values of 38.09°, 43.92°, 64.61°, and 77.14° correspond to hkl (111), (200), (220), and (311) silver fields are very comparable to the standard X-ray diffraction patterns from the Crystallography Open Database (COD) Entry 9013046. This discussion proves the synthesized AgNPs crystals have face-centered cubic (fcc) symmetry. The results of the XRD spectrum can also estimate the size of the AgNPs formed by the Debye-Scherrer equation (Equation 4). Based on the equation, the dimensions of the AgNPs formed were 5.11, 3.82, 7.98, and 7.16 nm. AgCl particles can occur due to the oxidation reaction of AgNPs when reacting with $Cl^-$ ions.[57]

$$D\ (nm) = \frac{K\lambda}{\beta cos\theta} \qquad \text{Equation 4}$$

D = crystal size (nm)
K = Scherer's constant (K=0.94)
Λ = X-ray wavelength (0.15418 Å)
β = Full Width at Half Maximum (FWHM) value (rad)
θ = diffraction angle (°)

Figure 8 shows Transmission Electron Spectroscopy (TEM) result and the size distribution of AgNPs-TK. The image shows that the particles are spherical in diameter in the 5–50 nm range. Differences in measurement results with PSA and TEM instruments may occur due to different treatments. The AgNPs-TK solution analyzed with PSA was not previously centrifuged so that the PSA/DLS instrument could detect the possibility of extracting particles in the solution. This difference can also originate from differences in the working principle of the equipment; the PSA instrument uses a laser beam to measure the size of hydrodynamic particles so that it ignores particle agglomeration. The particle size from the TEM image looks relatively uniform, consistent with the low polydispersity index obtained from the PSA results.

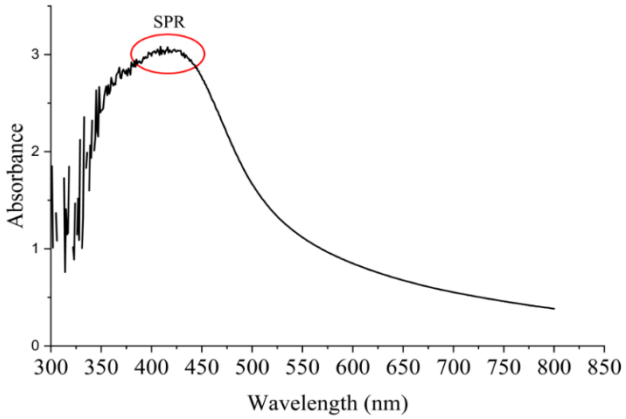


**Figure 4:** UV-Vis spectra of AgNPs-TK

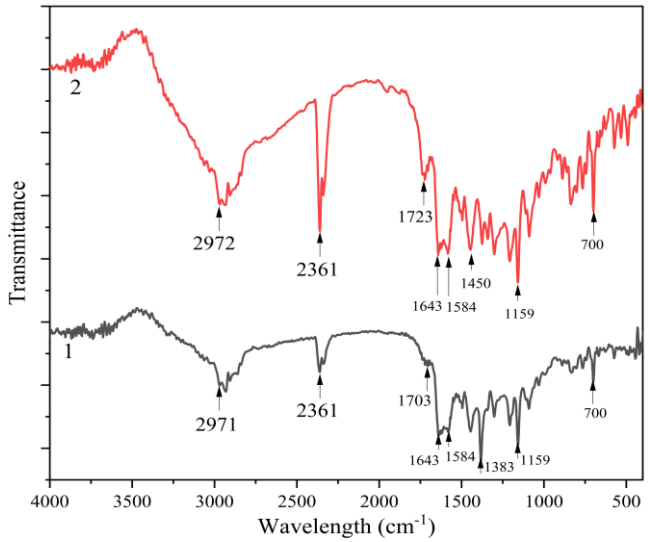


**Figure 5:** FTIR Spectra of (1) AgNPs-TK and (2) fingerroot/temu kunci extract

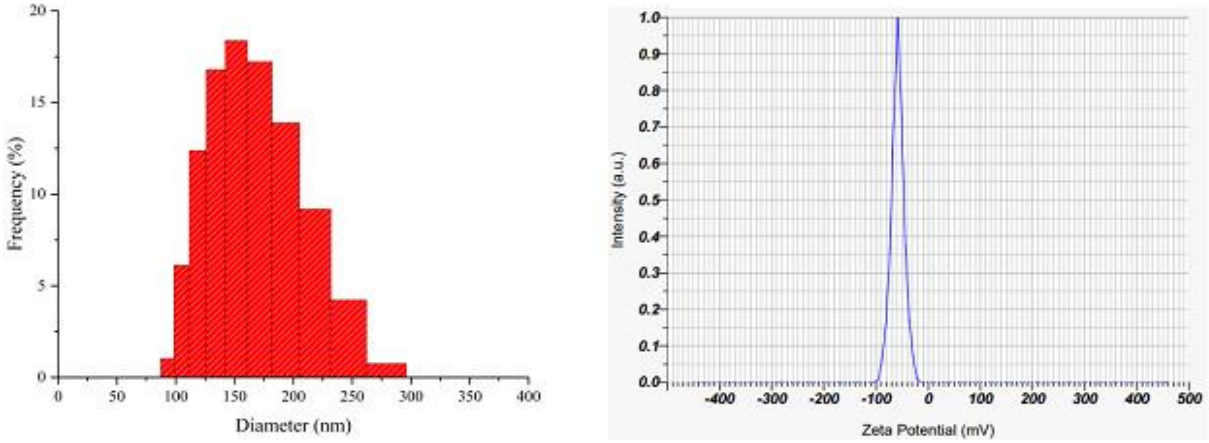


**Figure 6:** (a) PSA result of AgNPs-TK and (b) Zeta potential of AgNPs-TK

*Potential of AgNPs-TK as a sun protection substrate*

UV light is one of the leading causes of skin health problems in humans, such as skin redness and sunburn, the pathogenesis of which involves the induction of reactive oxygen species (ROS), DNA damage, skin cell death, and cancer. AgNPs have the potential to protect the skin from UV light. Research by Ho *et al.*[24] showed that AgNPs had an ability comparable to titanium oxide in protecting human keratinocyte cells from UV-B light. The study of Tyagi *et al.*[58] showed that AgNPs had better activity in protecting human skin cells from the harmful effects of UV-B light than $TiO_2$ and ZnO. However, AgNPs of 0.5 ppm and 50 ppm concentrations were proven unable to penetrate human skin.[59]

The Sun Protection Factor (SPF), according to the FDA, is a measure of how much solar energy (UV radiation) is required to produce a sunburn on protected (with sunscreen) skin relative to the amount of solar power needed to create a sunburn on unprotected skin. In our study, the in vitro SPF was measured spectrophotometrically. The spectrometric SPF method has the advantages of being simple, fast, potent, sensitive, selective, and suitable for in vitro determination of various sunscreens. The spectrophotometric SPF method could be a preliminary method for determining the SPF value of cosmetic products.[35,60] The SPF value produced by dried nanosilver particle products and measured for their SPFs is tabulated (Table 6). According to the FDA, an SPF of 2−12 can be considered minimum protection. SPF of 12−30 is categorized as moderate protection, and ≥30 is classified as high protection. The SPF value of AgNPs obtained using the spectrophotometric method has good results. Previous research of Tyagi *et al.*[58] showing SPF of AgNPs (~50 nm) is 1.207 at 25 ppm, 2.307 at 50 ppm, and 4.489 at 100 ppm.

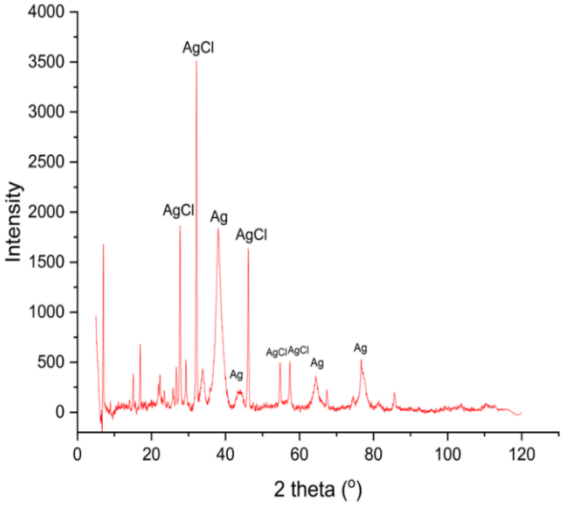


**Figure 7:** XRD spectra of AgNPs-TK

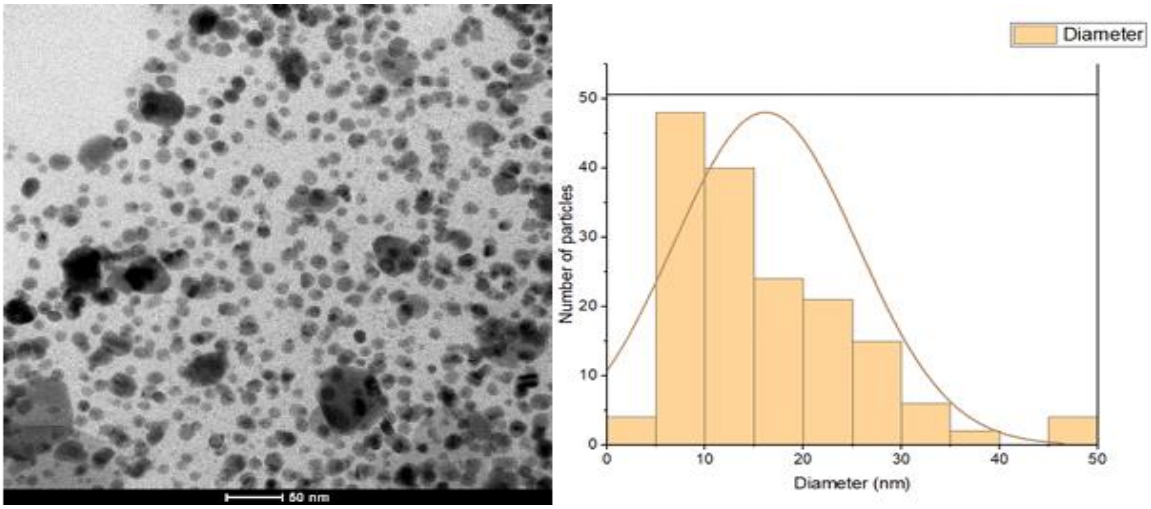


**Figure 8:** Transmission Electron Spectroscopy (TEM) result and particle size distribution of AgNPs-TK

## Conclusion

The rhizome extract of fingerroot (*C. rotunda*) is a potent reducing and stabilizing agent in the synthesis of AgNPs based on the characterization results from visible and infrared spectrophotometry, PSA, XRD, and TEM. In addition, the synthesis was optimized using the Box Behnken method to determine the most AgNPs produced using fingerroot extract as a bioreductive agent. The resulting products have the potential as a sun protection agent with a relatively high SPF value.

## Conflict of Interest

The authors declare no conflict of interest.

## Authors' Declaration

The authors hereby declare that the work presented in this article is original and that any liability for claims relating to the content of this article will be borne by them.

## Acknowledgements

This study was sponsored by the DGHE, Research and Technology, Ministry of Education, Culture, Research and Technology Indonesia, for financial support through the "RISET KOLABORASI INDONESIA (RKI) 2022" scheme under IPB University, Project No.3209/IT3.L1/PT.01.05/M.B/2022. The authors are grateful to National Research and Innovation Agency which has provided XRD and TEM facilities.

## References

1. Laurent S, Forge D, Port M, Roch A, Robic C, vander Elst L, Muller RN. Magnetic Iron Oxide Nanoparticles: Synthesis, Stabilization, Vectorization, Physicochemical Characterizations and Biological Applications. Chem Rev. 2008; 108: 2064–2110. Doi: 10.1021/cr068445e.
2. Khan I, Saeed K, Khan I. Nanoparticles: Properties, Applications and Toxicities. Arabian Journal of Chemistry. 2019; 12: 908–931, Doi: 10.1016/j.arabjc.2017.05.011.
3. Masum MI, Siddiqa MM, Ali KA, Zhang Y, Abdallah Y, Ibrahim E, Qiu W, Yan C, Li B. Biogenic Synthesis of Silver Nanoparticles Using *Phyllanthus Emblicafruit* Extract and Its Inhibitory Action against the Pathogen *Acidovorax*

*Oryzaestrain* RS-2 of Rice Bacterial Brown Stripe. Front Microbiol. 2019; 10, Doi: 10.3389/fmicb.2019.00820.
4. Shah MZ., Guan ZH, Din AU, Ali A, Rehman AU, Jan K, Faisal S, Saud S, Adnan M, Wahid F et al. Synthesis of Silver Nanoparticles Using *Plantago Lanceolata* Extract and Assessing Their Antibacterial and Antioxidant Activities. Sci Rep. 2021; 11, Doi: 10.1038/s41598-021-00296-5.
5. Sreelekha E, George B, Shyam A, Sajina N, Mathew BA. Comparative Study on the Synthesis, Characterization, and Antioxidant Activity of Green and Chemically Synthesized Silver Nanoparticles. Bionanoscience. 2021; 11: 489–496, Doi: 10.1007/s12668-021-00824-7.
6. Krithiga N, Rajalakshmi A, Jayachitra A. Green Synthesis of Silver Nanoparticles Using Leaf Extracts of *Clitoria Ternatea* and *Solanum Nigrum* and Study of Its Antibacterial Effect against Common Nosocomial Pathogens . Journal of Nanoscience. 2015; 2015: 1–8, Doi: 10.1155/2015/928204.
7. Barabadi H, Mojab F, Vahidi H, Marashi B, Talank N, Hosseini O, Saravanan M. Green Synthesis, Characterization, Antibacterial and Biofilm Inhibitory Activity of Silver Nanoparticles Compared to Commercial Silver Nanoparticles. Inorg Chem Commun. 2021; 129, Doi: 10.1016/j.inoche.2021.108647.
8. Zhang Y, Li M, Gao X, Chen Y, Liu T. Nanotechnology in Cancer Diagnosis: Progress, Challenges and Opportunities. J Hematol Oncol. 2019; 12: 1–13, Doi: 10.1186/s13045-019-0833-3.
9. Narayanan M, Divya S, Natarajan D, Senthil-Nathan S, Kandasamy S, Chinnathambi A, Alahmadi TA, Pugazhendhi A. Green Synthesis of Silver Nanoparticles from Aqueous Extract of *Ctenolepis Garcini* L. and Assess Their Possible Biological Applications. Process Biochemistry. 2021; 107: 91–99, Doi: 10.1016/j.procbio.2021.05.008.
10. Wei S, Wang Y, Tang Z, Xu H, Wang Z, Yang T, Zou T. A Novel Green Synthesis of Silver Nanoparticles by the Residues of Chinese Herbal Medicine and Their Biological Activities. RSC Adv. 2021; 11: 1411–1419, Doi: 10.1039/d0ra08287b.
11. Mallmann EJJ, Cunha FA, Castro BNMF, Maciel AM, Menezes EA, Fechine PBA. Atividade Antifúngica de Nanopartículas de Prata Obtidas Por Síntese Verde. Rev Inst Med Trop Sao Paulo. 2015; 57: 165–167, Doi: 10.1590/S0036-46652015000200011.
12. Oves M, Ahmar Rauf M, Aslam M, Qari HA, Sonbol H, Ahmad I, Sarwar Zaman G, Saeed M. Green Synthesis of Silver Nanoparticles by *Conocarpus Lancifolius* Plant Extract and Their Antimicrobial and Anticancer Activities. Saudi J Biol Sci. 2022; 29: 460–471. Doi: 10.1016/j.sjbs.2021.09.007.
13. Awad MA, al Olayan EM, Siddiqui MI, Merghani NM, Alsaif SSA llah, Aloufi AS. Antileishmanial Effect of Silver Nanoparticles: Green Synthesis, Characterization, in Vivo and in Vitro Assessment. Biomedicine and Pharmacotherapy. 2021; 137. Doi: 10.1016/j.biopha.2021.111294.
14. Mehwish HM, Rajoka MSR, Xiong Y, Cai H, Aadil RM, Mahmood Q, He Z, Zhu Q. Green Synthesis of a Silver Nanoparticle Using *Moringa Oleifera* Seed and Its Applications for Antimicrobial and Sun-Light Mediated Photocatalytic Water Detoxification. J Environ Chem Eng. 2021; 9. Doi: 10.1016/j.jece.2021.105290.
15. Zamarchi F, Vieira IC. Determination of Paracetamol Using a Sensor Based on Green Synthesis of Silver Nanoparticles in Plant Extract. J Pharm Biomed Anal. 2021; 196. Doi: 10.1016/j.jpba.2021.113912.
16. Chinnasamy G, Chandrasekharan S, Koh TW, Bhatnagar S. Synthesis, Characterization, Antibacterial and Wound Healing Efficacy of Silver Nanoparticles From *Azadirachta Indica*. Front Microbiol. 2021; 12. Doi: 10.3389/fmicb.2021.611560.
17. Iravani S, Korbekandi H, Mirmohammadi S v, Zolfaghari B. Synthesis of Silver Nanoparticles: Chemical, Physical and Biological Methods, Res Pharm Sci. 2014; 9: 385–406. https://pubmed.ncbi.nlm.nih.gov/26339255.
18. Liu YC, Lin LH. New Pathway for the Synthesis of Ultrafine Silver Nanoparticles from Bulk Silver Substrates in Aqueous Solutions by Sonoelectrochemical Methods. Electrochem commun. 2004; 6: 1163–1168, Doi: 10.1016/j.elecom.2004.09.010.
19. Solanki JN, Murthy ZVP. Highly Monodisperse and Sub-Nano Silver Particles Synthesis via Microemulsion Technique. Colloids Surf A Physicochem Eng Asp. 2010; 359: 31–38. Doi: 10.1016/j.colsurfa.2010.01.058.
20. Jara N, Milán NS, Rahman A, Mouheb L, Boffito DC, Jeffryes C, Dahoumane SA. Photochemical Synthesis of Gold and Silver Nanoparticles-a Review. Molecules; 2021: 26. Doi: 10.3390/molecules26154585.
21. Wang B, Zhuang X, Deng W, Cheng B. Microwave-Assisted Synthesis of Silver Nanoparticles in Alkalic Carboxymethyl Chitosan Solution. Engineering. 2010; 02: 387–390. Doi: 10.4236/eng.2010.25050.
22. Filip GA, Moldovan B, Baldea I, Olteanu D, Suharoschi R, Decea N, Cismaru CM, Gal E, Cenariu M, Clichici S, et al. UV-Light Mediated Green Synthesis of Silver and Gold Nanoparticles Using Cornelian Cherry Fruit Extract and Their Comparative Effects in Experimental Inflammation. J Photochem Photobiol B. 2019; 191: 26–37. Doi: 10.1016/j.jphotobiol.2018.12.006.
23. Huang L, Zhai ML, Long, DW, Peng J, Xu L, Wu GZ, Li JQ, Wei GS. UV-Induced Synthesis, Characterization and Formation Mechanism of Silver Nanoparticles in Alkalic Carboxymethylated Chitosan Solution. Journal of Nanoparticle Research. 2008; 10: 1193–1202. Doi: 10.1007/s11051-007-9353-0.
24. Ho YY, Sun DS, Chang HH. Silver Nanoparticles Protect Skin from Ultraviolet B-Induced Damage in Mice. Int J Mol Sci. 2020; 21: 1–11. Doi: 10.3390/ijms21197082.
25. Palanki R, Arora S, Tyagi N, Rusu L, Singh AP, Palanki S, Carter JE, Singh S. Size Is an Essential Parameter in Governing the UVB-Protective Efficacy of Silver Nanoparticles in Human Keratinocytes. BMC Cancer. 2015; 15: 1–7. Doi: 10.1186/s12885-015-1644-8.
26. Halilu EM, Ngweh VA, Airemwen CO. Green Synthesis of Silver Nanoparticles from Parinari curatellifolia Methanol Stem Bark Extract and Evaluation of Antioxidant and Antimicrobial Activities. Trop. J. Nat. Prod. Res. 2023; 7(3):2498–2505
27. Ahmed S, Ahmad M, Swami BL, Ikram S. A Review on Plants Extract Mediated Synthesis of Silver Nanoparticles for Antimicrobial Applications: A Green Expertise. J Adv Res. 2016; 7: 17–28. Doi: 10.1016/j.jare.2015.02.007.
28. Tarannum N, Divya, Gautam YK. Facile Green Synthesis and Applications of Silver Nanoparticles: A State-of-the-Art Review. RSC Adv. 2019; 9: 34926–34948. Doi: 10.1039/c9ra04164h.
29. Ewon K, Bhagya AS. A Review on Golden Species of *Zingiberaceae* Family around the World: Genus Curcuma. Afr J Agric Res. 2019; 14: 519–531. Doi: 10.5897/ajar2018.13755.
30. Gul P, Bakht J. Antimicrobial Activity of Turmeric Extract and Its Potential Use in Food Industry. J Food Sci Technol. 2015; 52: 2272–2279. Doi: 10.1007/s13197-013-1195-4.
31. Dairaku I, Han Y, Yanaka N, Kato N. Inhibitory Effect of Curcumin on IMP Dehydrogenase, the Target for Anticancer and Antiviral Chemotherapy Agents. Biosci Biotechnol Biochem. 2010; 74: 185–187. Doi: 10.1271/bbb.90568.
32. Khandelwal RSUP, Reddy AHM. An Antifungal Agent in Plant Tissue Culture Studies. International Journal of Engineering Science and Technology. 2011; 3: 7899–7904. https://www.researchgate.net/publication/302997674

33. Patra D, el Kurdi R. Curcumin as a Novel Reducing and Stabilizing Agent for the Green Synthesis of Metallic Nanoparticles. Green Chem Lett Rev. 2021; 14: 474–487. Doi: 10.1080/17518253.2021.1941306.
34. Alsammarraie FK, Wang W, Zhou P, Mustapha A, Lin M. Green Synthesis of Silver Nanoparticles Using Turmeric Extracts and Investigation of Their Antibacterial Activities. Colloids Surf B Biointerfaces. 2018; 171:398–405. Doi: 10.1016/j.colsurfb.2018.07.059.
35. Dutra EA, da Costa E Oliveira DAG, Kedor-Hackmann ERM, Miritello Santoro MIR. Determination of Sun Protection Factor (SPF) of Sunscreens by Ultraviolet Spectrophotometry. Revista Brasileira de Ciencias Farmaceuticas/Brazilian Journal of Pharmaceutical Sciences. 2004; 40: 381–385. Doi: 10.1590/S1516-93322004000300014.
36. Zeng Y, Hu R, Wang L, Gu D, He J, Wu SY, Ho HP, Li X, Qu J, Gao BZ, et al. Recent Advances in Surface Plasmon Resonance Imaging: Detection Speed, Sensitivity, and Portability. Nanophotonics. 2017; 6: 1017–1030. Doi: 10.1515/nanoph-2017-0022.
37. Oyagi MO, Michira IN, Guto P, Baker PGL, Kamau G, Iwuoha I. Polydisperse Low Diameter 'Non-Toxic' Silver Nanoparticles Encapsulated by Rooibos Tea Templates. Nano Hybrids. 2014; 8: 57–72. Doi: 10.4028/www.scientific.net/nh.8.57.
38. Arshad H, Sami MA, Sadaf S, Hassan U. *Salvadora Persica* Mediated Synthesis of Silver Nanoparticles and Their Antimicrobial Efficacy. Sci Rep. 2021; 11, Doi: 10.1038/s41598-021-85584-w.
39. Anandalakshmi K, Venugobal J, Ramasamy V. Characterization of Silver Nanoparticles by Green Synthesis Method Using *Pedalium Murex* Leaf Extract and Their Antibacterial Activity. Applied Nanoscience (Switzerland). 2016; 6: 399–408. Doi: 10.1007/s13204-015-0449-z.
40. Aravinthan A, Govarthanan M, Selvam K, Praburaman L, Selvankumar T, Balamurugan R, Kamala-Kannan S, Kim JH. Sunroot Mediated Synthesis and Characterization of Silver Nanoparticles and Evaluation of Its Antibacterial and Rat Splenocyte Cytotoxic Effects. Int J Nanomedicine. 2015; 10: 1977–1983. Doi: 10.2147/IJN.S79106.
41. Selvam K, Sudhakar C, Govarthanan M, Thiyagarajan P, Sengottaiyan A, Senthilkumar B, Selvankumar T. Eco-Friendly Biosynthesis and Characterization of Silver Nanoparticles Using *Tinospora Cordifolia* (Thunb.) *Miers* and Evaluate Its Antibacterial, Antioxidant Potential. J Radiat Res Appl Sci. 2017; 10: 6–12. Doi: 10.1016/j.jrras.2016.02.005.
42. Dahoumane SA, Yéprémian C, Djédiat C, Couté A, Fiévet F, Coradin T, Brayner R. A Global Approach of the Mechanism Involved in the Biosynthesis of Gold Colloids Using Micro-Algae. Journal of Nanoparticle Research. 2014; 16: 1–12. Doi: 10.1007/s11051-014-2607-8.
43. Azmi SNH, Al-Jassasi BMH, Al-Sawafi HMS, Al-Shukaili SHG, Rahman N, Nasir M. Optimization for Synthesis of Silver Nanoparticles through Response Surface Methodology Using Leaf Extract of *Boswellia Sacra* and Its Application in Antimicrobial Activity. Environ Monit Assess. 2021; 193. Doi: 10.1007/s10661-021-09301-w.
44. Ibrahim S, Ahmad Z, Manzoor MZ, Mujahid M, Faheem Z, Adnan A. Optimization for Biogenic Microbial Synthesis of Silver Nanoparticles through Response Surface Methodology, Characterization, Their Antimicrobial, Antioxidant, and Catalytic Potential. Sci Rep. 2021; 11. Doi: 10.1038/s41598-020-80805-0.
45. Czyrski A, Sznura J. The Application of Box-Behnken-Design in the Optimization of HPLC Separation of Fluoroquinolones. Sci Rep. 2019; 9: 1–10. Doi: 10.1038/s41598-019-55761-z.
46. Mathew S, Prakash A, Radhakrishnan EK. Sunlight Mediated Rapid Synthesis of Small Size Range Silver Nanoparticles Using *Zingiber Officinale* Rhizome Extract and Its Antibacterial Activity Analysis. Inorganic and Nano-Metal Chemistry. 2018; 48: 139–145. Doi: 10.1080/24701556.2017.1373295.
47. Sakamoto M, Fujistuka M, Majima T. Light as a Construction Tool of Metal Nanoparticles: Synthesis and Mechanism. Journal of Photochemistry and Photobiology C: Photochemistry Reviews. 2009; 10: 33–56. Doi: 10.1016/j.jphotochemrev.2008.11.002.
48. Darroudi M, Ahmad MB, Zak AK, Zamiri R, Hakimi M. Fabrication and Characterization of Gelatin Stabilized Silver Nanoparticles under UV-Light. Int J Mol Sci. 2011; 12: 6346–6356. Doi: 10.3390/ijms12096346.
49. Shet A, Shetty KV. Photocatalytic Degradation of Phenol Using Ag Core-$TiO_2$ Shell (Ag@$TiO_2$) Nanoparticles under UV Light Irradiation. Environmental Science and Pollution Research. 2016; 23: 20055–20064. Doi: 10.1007/s11356-015-5579-z.
50. Kamat P v, Flumiani M, Hartland G v. Picosecond Dynamics of Silver Nanoclusters. Photoejection of Electrons and Fragmentation. Journal of Physical Chemistry B. 1998; 102: 3123–3128. Doi: 10.1021/jp980009b.
51. Kuthirummal N, Dean A, Yao C, Risen W. Photo-Formation of Gold Nanoparticles: Photoacoustic Studies on Solid Monoliths of Au(III)-Chitosan-Silica Aerogels. Spectrochim Acta A Mol Biomol Spectrosc. 2008; 70: 700–703. Doi: 10.1016/j.saa.2007.09.011.
52. Ahmad N, Ang BC, Amalina MA, Bong CW. Influence of Precursor Concentration and Temperature on the Formation of Nanosilver in Chemical Reduction Method. Sains Malays. 2018; 47: 157–168. Doi: 10.17576/jsm-2018-4701-19.
53. Ball RC, Weitz DA, Witten TA, Leyvraz F. Universal Kinetics in Reaction-Limited Aggregation. Phys Rev Lett. 1987; 58: 274–277. Doi: 10.1103/PhysRevLett.58.274.
54. Traiwatcharanon P, Timsorn K, Wongchoosuk C. Flexible Room-Temperature Resistive Humidity Sensor Based on Silver Nanoparticles. Mater Res Express. 2017; 4. Doi: 10.1088/2053-1591/aa85b6.
55. Sun L, Zhang Z, Dang H. A Novel Method for Preparation of Silver Nanoparticles. Mater Lett. 2003; 57: 3874–3879. Doi: 10.1016/S0167-577X(03)00232-5.
56. Meléndrez MF, Cárdenas G, Arbiol J. Synthesis and Characterization of Gallium Colloidal Nanoparticles. J Colloid Interface Sci. 2010; 346: 279–287. Doi: 10.1016/j.jcis.2009.11.069.
57. Garg S, Rong H, Miller CJ, Waite TD. Oxidative Dissolution of Silver Nanoparticles by Chlorine: Implications to Silver Nanoparticle Fate and Toxicity. Environ Sci Technol. 2016; 50: 3890–3896. Doi: 10.1021/acs.est.6b00037.
58. Tyagi N, Srivastava SK, Arora S, Omar Y, Ijaz ZM, AL-Ghadhban A, Deshmukh SK, Carter JE, Singh AP, Singh S. Comparative Analysis of the Relative Potential of Silver, Zinc-Oxide and Titanium-Dioxide Nanoparticles against UVB-Induced DNA Damage for the Prevention of Skin Carcinogenesis. Cancer Lett. 2016; 383: 53–61. Doi: 10.1016/j.canlet.2016.09.026.
59. Kokura S, Handa O, Takagi T, Ishikawa T, Naito Y, Yoshikawa T. Silver Nanoparticles as a Safe Preservative for Use in Cosmetics. Nanomedicine. 2010; 6: 570–574. Doi: 10.1016/j.nano.2009.12.002.
60. Yang SI, Liu S, Brooks GJ, Lanctot Y, Gruber J v. Reliable and Simple Spectrophotometric Determination of Sun Protection Factor: A Case Study Using Organic UV Filter-Based Sunscreen Products. J Cosmet Dermatol. 2018; 17: 518–522. Doi: 10.1111/jocd.12390.